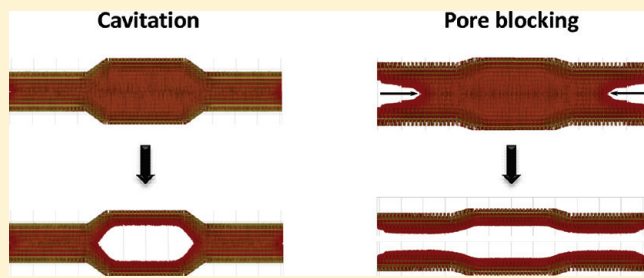


On The Cavitation and Pore Blocking in Cylindrical Pores with Simple Connectivity

Phuong T. M. Nguyen, D. D. Do,* and D. Nicholson

School of Chemical Engineering, University of Queensland, St. Lucia, Queensland 4072, Australia

ABSTRACT: We present a grand canonical Monte Carlo (GCMC) simulation of argon adsorption in connected cylindrical pores at 87.3 K. A number of pore models are constructed from various components: finite cylinder, finite cone, and flat surface. In the case of two cylinders of different sizes connected to each other with open ends, the adsorption isotherm can be described by a combination of two independent pores, the smaller of which is opened at both ends while the larger one is closed at one end. The adsorption isotherm depends on the relative size between the two sections of the connected pore. In the case of a cavity connected to the bulk surrounding gas via one or two narrower cylindrical necks, the phenomenon of either pore blocking or cavitation is observed, depending on the relative size between the neck and the cavity. If the neck size is smaller than a critical size, D_c , we observe cavitation, while pore blocking is observed when it is greater than D_c . This is due to the dominance of one of two mechanisms for removal of the adsorbates: either the receding of the menisci or the stretching of the fluid in the cavity. We also explore the effects of neck length and cavity length on the adsorption isotherm and conclude that while the neck length has a negligible effect on cavitation, it is of considerable importance when pore blocking occurs, because this process is controlled by the formation and movement of the meniscus in the pore neck. The effect of cavity length is found to be negligible in both cases.



1. INTRODUCTION

Due to the significant development of new materials with various shapes and sizes in recent years and the potential for their applications in chemical and energy industries, there is a pressing need for improved characterization of pore morphology and pore size. These parameters are mainly derived from the analysis of an experimental adsorption isotherm. Since condensation and evaporation are sensitive to pore size in the mesopore size range and to pore structure, the portions of the isotherm in the regions of condensation and evaporation are analyzed for the required parameters. At a sufficiently low temperature, the isotherm in these regions exhibits a hysteresis loop enclosing stable and metastable states. The shape and size of this hysteresis loop are complex functions of the temperature, pore size, pore shape, pore affinity, and type of the adsorbate.¹ The origin of the hysteresis phenomenon in adsorption has been investigated by classical theory and by simulation over the last century, but discrepancies remain.

In a 1938 paper, Cohan proposed that for pores open at both ends, condensation is controlled by a cylindrical meniscus, whereas evaporation of the liquid would occur from a hemispherical meniscus, leading to different values of P/P_0 for condensation and evaporation.^{1,2} Foster suggested³ that hysteresis is due to the delay of the meniscus formation. Later Saam and Cole produced a statistical mechanical argument to show that hysteresis could be attributed to the limit of stability and metastability of an adsorbed multilayer film in a cylindrical pore. In this theory, condensation occurs at a critical film thickness, t_c ,

when the cylindrical adsorbed film reaches its thermodynamic stability limit, which depends on both substrate and capillary forces.⁴ Broekhoff and de Boer, in a series of papers, stressed the importance of the adsorbent field and discussed the role of film thickness and curvature in detail.^{5–7} Their theory, like that of Saam and Cole,⁴ captures the essential mechanism of pore condensation and hysteresis.

An alternative mechanism for the source of hysteresis, originally proposed by McBain, is known as the “ink bottle model” in which condensate in a closed cavity is trapped by a narrow neck and this fluid remains trapped until the vapor pressure is low enough for the adjacent narrow pore to empty. This basic idea has been extended and applied to networks of interconnected pores by combining it with percolation theory^{8–10} so that desorption becomes dependent on the probability of finding a path empty of condensate that connects to the external vapor phase.

Recent molecular dynamics simulations in various pore geometries have shown that the McBain theory is not universally valid because the confined fluid in the cavity can evaporate via diffusion through the narrow neck.¹¹ Therefore, the hysteresis loop in this case is not caused by a pore blocking mechanism. Similar conclusions can also be drawn from the scanning experiment results of Everett and co-workers.^{12,13} Subsequently it has

Received: July 18, 2011

Revised: September 5, 2011

Published: September 09, 2011

been suggested that pore blocking does not occur when the pore neck is small (where cavitation occurs) but can occur when the neck is comparable in size to the cavity.^{14–16} The switching of mechanism from pore blocking to cavitation can be caused not only by variations in the relative size of the neck and the cavity but also by change of the temperature. This opens the possibility of tuning the experimental conditions in order to characterize the pore neck size distribution.^{14,17} Recently, Fan et al.¹⁸ have studied slit-shaped ink-bottle pores and have suggested that local compressibility provides a measure of the cohesiveness of the fluid prior to evaporation.

Although there are many classical (including DFT) and molecular simulation investigations of condensation and evaporation (and hysteresis) in adsorption, our understanding of the microscopic origin of these phenomena and of pore blocking and cavitation in a connected pore is still rather limited. In our previous work, we have shown that hysteresis in a single cylindrical pore can be observed when the pore size exceeds a critical value. We have also shown the importance of distinguishing the hysteresis loop for a pore with connectivity and for a combination of individual pores of different sizes because these hysteresis loops have similar size and shape.¹⁹ The aims of this work are to investigate the behavior of the hysteresis loop in pores with simple connectivity and to determine the microscopic origin of condensation/evaporation in a connected pore and compare these with independent cylindrical pores. We also study systematically the cavitation–pore blocking phenomena in a cavity connected to the bulk surrounding gas via one or two narrower necks. The effects of the diameter and length of the cavity and the neck on the adsorption behavior of the pore are also explored.

2. INTERACTION ENERGY AND PORE MODELS

To describe the fluid–fluid interaction energy of argon, we use the 12–6 Lennard-Jones equation with the following molecular parameters: $\sigma_{\text{ff}} = 0.3405 \text{ nm}$ and $\varepsilon_{\text{ff}}/k = 119.8 \text{ K}$.^{20,21}

The connected pore models in this paper are constructed from various components, finite cylindrical pore, finite truncated cone, and flat surface, and differ from many other suggested models for ink-bottle pores, which comprise one spherical cavity connected by a cylindrical neck to the external phase. Different types of connected pores are obtained by varying the dimensions of these components and their sequence of connection. This provides a very flexible means of studying cavitation and pore blocking as a function of the system parameters and operating conditions. We can even model a spherical cavity with a cylindrical neck using these elements since by setting the diameter and length of the cavity to be equal, the internal cavity will become practically spherical after the initial stage of adsorption.

The solid–fluid potential energy of an adsorbate with a connected pore is the sum of the solid–fluid potential energies contributed by each section making up the pore:

$$\varphi_{i,S} = \varphi_{i,S_1} + \varphi_{i,S_2} + \varphi_{i,S_3} + \dots \quad (1)$$

All sections of the pore are three-layer graphitic objects. The solid–fluid interactions between an adsorbate and a finite cylindrical pore or a closed end surface have been described in our previous work.¹⁹ In the closed end surface constructed of argon molecules, the solid–fluid potential interaction of an adsorbate inside the pore and this surface is modeled with Steele 10–4–3 equation²² in which the distance between two

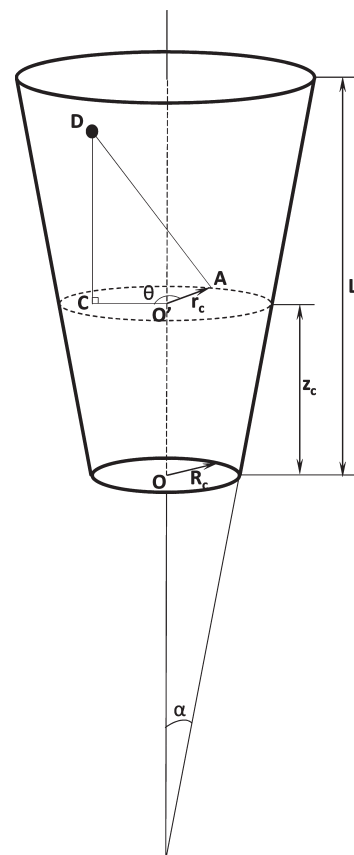


Figure 1. The schematic diagram of a truncated cone and an adsorbate inside the truncated cone.

layers is equal to the collision diameter of argon (σ_{ff}) and the surface density is equal to that of liquid argon confined in a cylindrical pore at 87 K: $\rho_s^{\text{Ar}} = 8.2 \text{ nm}^{-2}$ (corresponding to a density of 40 kmol/m^3).

For the junction between two cylindrical sections, we use a truncated cone. The solid–fluid potential energy between an adsorbate and a single-wall truncated cone is given by the following equation (a detailed derivation and a definition of the integral are given in Appendix 1):

$$\varphi_{sf} = \frac{4\varepsilon_{sf}\rho_s}{\cos \alpha} \sum_{n=3,6} a_n \sigma_{sf}^{2n} \int_0^{2\pi} I(\theta, r_c, z_c, n, R_c, L_c, \alpha) d\theta \quad (2)$$

where σ_{sf} and ε_{sf} are solid–fluid molecular parameters estimated from the Lorentz–Berthelot rule; ρ_s is the surface density of solid atoms on the pore wall (for a graphene layer $\rho_s = 38.2 \text{ nm}^{-2}$); a_n is a constant ($a_3 = 1$ and $a_6 = -1$); R_c and L_c are the radius of the small end and the length of the cone, respectively; r_c is the radial distance from the pore axis to a point A on the pore wall; z_c is the axial distance from the small end; and α is the angle of the truncated cone, which is shown in Figure 1. The potential energy of a multilayer truncated cone is the summation of the potentials of concentric truncated cones with $R_c^i = R_c + i\Delta$ ($i = 0, 1, \dots$) where Δ is the distance between two adjacent graphene layers ($\Delta = 0.3354 \text{ nm}$).

We have studied four models for connected pores (shown in Figure 2).

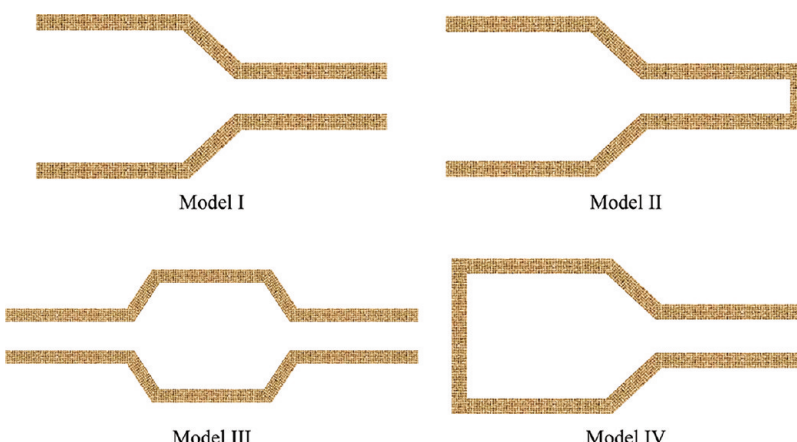


Figure 2. Four models of the connected pore.

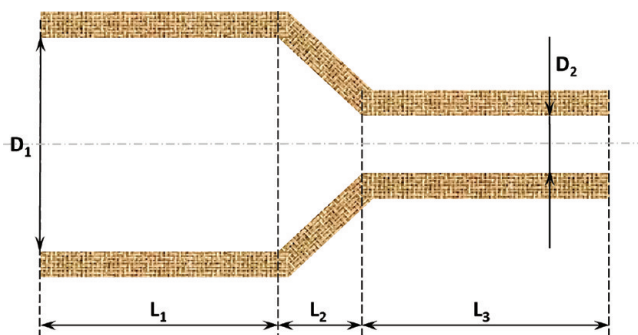


Figure 3. Pore model I.

- Model I: A connected pore with two open ends, constructed by combining two cylinders together with a truncated cone.
- Model II: Same as model I, but with the smaller end closed.
- Model III: Formed by joining a large cylinder with two smaller cylinders at two ends by two truncated cones.
- Model IV: An ink-bottle pore; the same as model I, but with the larger end closed.

The first two models are used to investigate the relationship between the adsorption isotherms of a simple connected pore and those of independent cylindrical pores. The third and the fourth models are used to study cavitation and pore-blocking phenomena.

3. MONTE CARLO SIMULATION

To acquire the data in the grand canonical Monte Carlo (GCMC) simulation, we use at least 100 000 cycles for the system to reach equilibrium and another 20 000 cycles for the statistics collection. Each cycle has 1000 displacement moves and exchanges, which include insertion and deletion with equal probability. In the equilibrium step, the maximum initial displacement length is half of the smallest dimension of the simulation box and is adjusted at the end of every cycle such that the acceptance ratio of displacement falls between 25% and 75%. The cutoff radius is chosen as half of the largest dimension of the simulation box.

The excess amount is defined as the difference between the amount in the pore and the hypothetical amount of gas occupying the accessible volume at the same density as the bulk gas. The pore density is defined as the excess amount per unit accessible volume of the pore or that section.²³

$$\rho_{\text{excess}} = \frac{N_{\text{excess}}}{V_{\text{acc}}} = \frac{\langle N \rangle - \rho_G V_{\text{acc}}}{V_{\text{acc}}} \quad (3)$$

where V_{acc} is the accessible volume of the pore in which the solid–fluid potential is nonpositive,²⁴ and ρ_G is the bulk gas density.

4. RESULTS AND DISCUSSION

4.1. Pore Model I. Figure 3 shows the dimensions of this pore. The important parameters are the sizes and lengths of the two cylinders.

Figure 4 shows the adsorption isotherms of argon at 87.3 K for this pore and the contributions from each section of the pore. The dimensions used in the computation of these isotherms are $D_1 = 6.0$ nm, $D_2 = 4.8$ nm, $L_1 = L_3 = 6.81$ nm, and $L_2 = 2.0$ nm. The adsorption isotherms of independent finite cylindrical pores of 4.8 and 6.0 nm and the isotherm of a closed end cylindrical pore (diameter 6 nm) whose closed end is a Steele surface of confined liquid argons are also shown in the same figure. These independent pores have the same length as the respective sections of the connected pore.

The isotherm of the connected pore exhibits two hysteresis loops with the first loop associated with the filling and emptying of the narrower section and the second loop (very small in size but detectable) associated with those of the wider section of the pore. Comparing these loops with the corresponding loops of the two open-ended independent pores (shown in Figure 4B), we see that the first hysteresis (associated with the narrower section) is unaffected by the presence of the wider section because the condensation and evaporation pressures are the same as those of the independent pore. On the other hand, the second loop of the isotherm is very different from that of the independent open-end pore of 6 nm due to the influence of adsorbates in the smaller section of the pore. To explain this, let us consider the mechanism of adsorption (see Figure 5). At low pressures, layering occurs in both sections of the pore, with thicker layers in the narrower section because the solid–fluid potential is deeper than

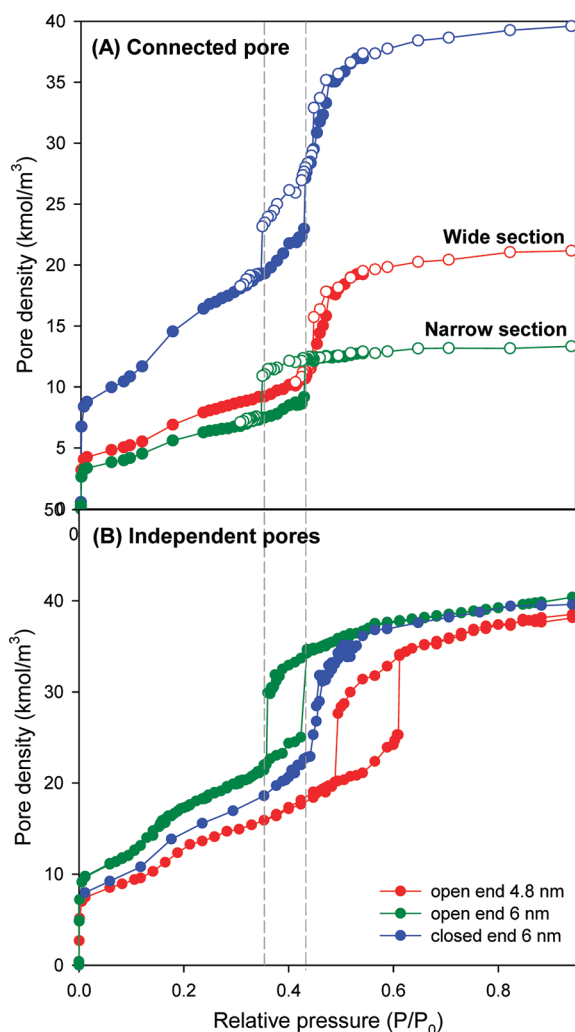


Figure 4. Adsorption isotherms of (A) the pore model I with contributions of each section ($D_1 = 6.0$ nm; $D_2 = 4.8$ nm) and (B) independent finite cylindrical pores of 4.8 and 6.0 nm (open end and closed end) having the same length as the respective sections of the connected pore.

in the larger section (Figure 5A). When the condensation pressure in the narrower section is reached, condensation occurs, but this process is unaffected by the presence of the thin adsorbed film in the wider section (Figure 5B). As pressure is further increased two processes occur in the wider section: (i)

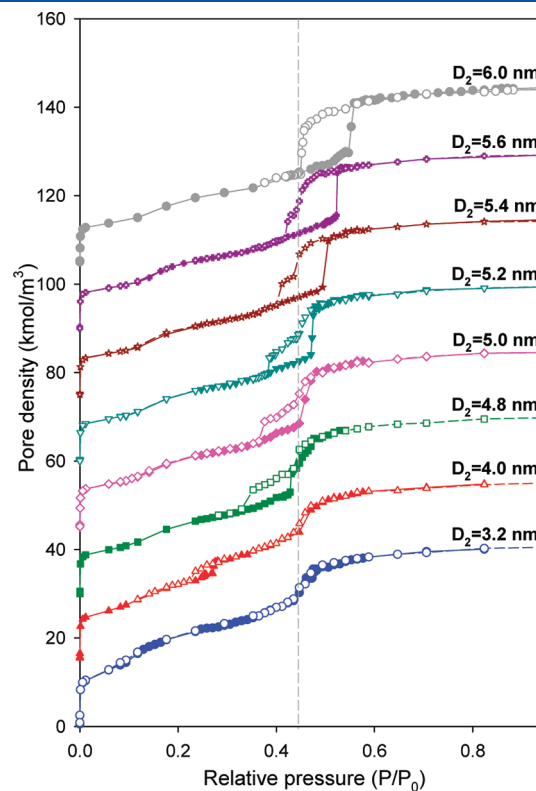


Figure 6. Adsorption isotherm of pore model I with the same size for the wide section ($D_1 = 6$ nm) and different sizes of the narrow section (D_2). The isotherms of pores with the diameter of the narrow section (D_2) equal to 4.0, 4.8, 5.0, 5.2, 5.4, 5.6, and 6.0 nm are shifted up 15, 30, 45, 60, 75, 90, and 105 kmol/m³, respectively. Closed symbols represent adsorption branches while open symbols represent desorption branches.

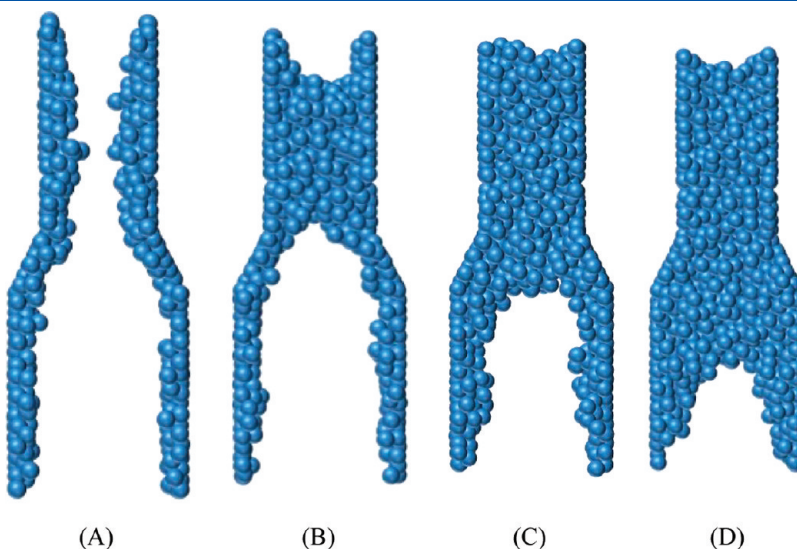


Figure 5. Schematic illustration of the pore filling process (A → D) and pore emptying process (D → A) in a model I connected pore.

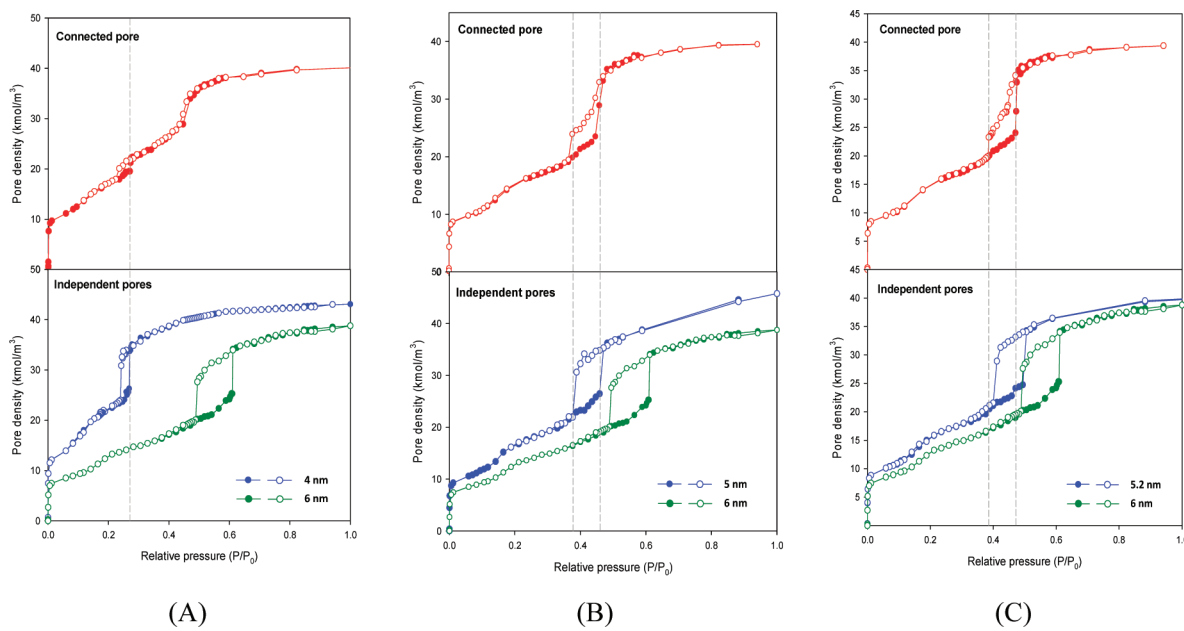


Figure 7. Adsorption isotherms for a connected pore (pore model I) in comparison with those for independent finite cylindrical pores. The diameters are (A) 4 and 6.0 nm, (B) 5 and 6 nm, and (C) 5.2 and 6 nm.

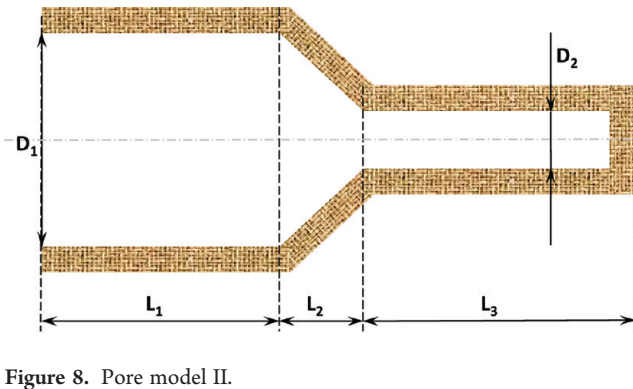


Figure 8. Pore model II.

adsorbed film on the cylindrical wall gets thicker and (ii) the meniscus formed at the junction between the two sections (from the condensation in the narrower section) advances into the wider section (Figure 5C,D). It is this second process that enhances the adsorption compared with that of the independent pore, causing the “condensation” in the wider section to occur at a lower pressure (see Figure 4A). It must be stressed that filling of the larger section is not a first-order transition, but rather it is a filling process that combines the advance of the meniscus and growth of the adsorbed layer. The first process dominates because of the greater fluid–fluid interaction in the neighborhood of the hemispherical meniscus than the fluid–fluid interaction near the cylindrical adsorbed layer. Upon decreasing the pressure, the condensed fluid in the wider section of the pore evaporates at a pressure lower than the evaporation pressure of the corresponding independent pore, due not only to the stabilizing effects of the condensed fluid in the smaller section but also to the number of openings to the surroundings being reduced to one, compared with two in the case of the independent open-ended pore. Further reduction in pressure results in evaporation from the smaller section at the same pressure as the corresponding

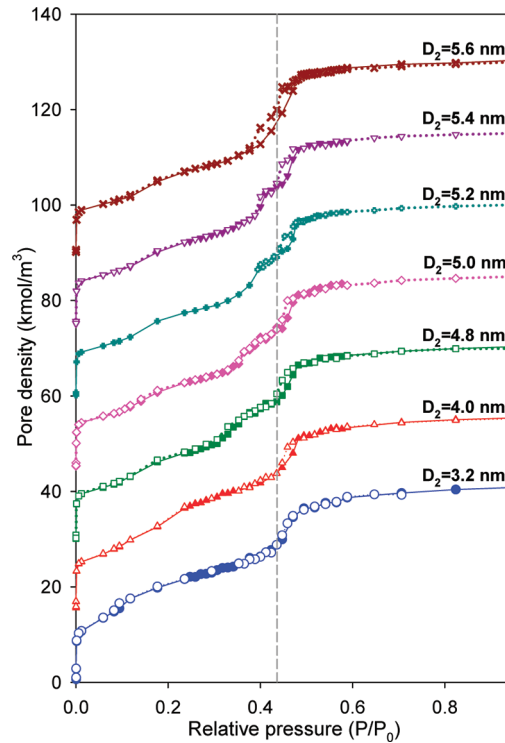


Figure 9. Adsorption isotherm for Ar at 87.3 K in pore model II. The wide pore has a fixed diameter ($D_1 = 6$ nm), and the narrow pore diameter is varied from $D_2 = 3.2$ to 5.6 nm. The isotherms for the pore diameters $D_2 = 4.0\text{--}5.6$ nm are shifted up 15, 30, 45, 60, 75, and 90 kmol/m³, respectively. Closed symbols are for adsorption branches and open symbols for desorption branches.

independent pore, because the smaller section is exposed to the adsorptive at both ends. It is worth noting that the condensation and evaporation from the wider section of the pore is similar to

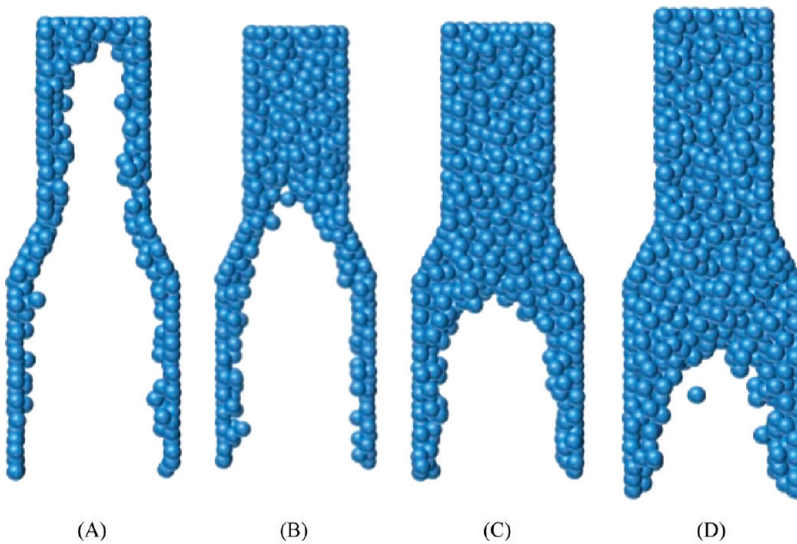


Figure 10. The schematic of pore filling ($A \rightarrow D$) and pore emptying ($D \rightarrow A$) processes in a model II connected pore.

that from cylindrical pore closed by a Steele surface constructed from confined liquid argon (blue symbols in Figure 4B).¹⁹

Figure 6 shows the adsorption isotherms of the connected pore with various sizes (3.2–6 nm) of the narrow section with the other dimensions kept constant: $D_1 = 6$ nm, $L_1 = L_3 = 6.81$ nm, and $L_2 = 2.0$ nm. Depending on the relative size of the two sections, the adsorption isotherm changes from reversible to one with hysteresis in which two hysteresis loops can occur. When the difference in size between the narrow and wide sections is reduced the two loops become closer and finally merge to a single loop when the two sections are equal in size (as expected for a single cylindrical pore of 6 nm). We illustrate this further this by choosing diameters of 4, 4.8, and 5.2 nm for the narrow section. The isotherms of these connected pores and those of the corresponding independent cylindrical pores with open ends are shown in Figure 7.

When the difference between the size of the two sections is large (Figure 7A), the adsorption isotherm clearly shows a consecutive filling of the narrow and wide sections. The isotherms for the corresponding independent pores have widely separated hysteresis loops. Therefore, when condensation in the narrow section has occurred, the state of the wide section is still far below the incipient condensation. When the pressure increases further, filling of the wide section occurs, and adsorption is dominated by the advancing meniscus resulting from the condensation in the narrow section rather than the growth of the adsorbed layer on the walls of the wide section. On decreasing the pressure, evaporation from the narrow section occurs at a lower pressure than filling because the molecules at the center of the meniscus are the most weakly held (having fewer neighbors) and are desorbed first.¹⁹

When the two sections are closer in size (Figure 7B), there is just one steep increase in the amount adsorbed indicating that condensation happens in the two sections simultaneously. The bottom curves in Figure 7B show that the hysteresis loops of the corresponding independent cylindrical pores are now close to each other. Therefore, when the condensation pressure of the narrow section is reached, the fluid in the wider section is almost at its condensation state, and a small increase in pressure results in condensation in the wide section. Along the

desorption path, pore emptying first occurs from the open end of the wide section via a process of meniscus movement toward the narrow section. When the pressure is further decreased, evaporation occurs in the narrower section at a lower pressure compared with its condensation pressure resulting in a double hysteresis loop because the fluid remains in the metastable state, which is stabilized by the fluid–fluid interactions within the condensate.

When the size of the two sections is very close (Figure 7C), the behavior of the adsorption isotherm is similar to that in Figure 7B. However, the condensation and evaporation in the narrow section shift slightly to lower pressures compared with those of the independent pore. This is due to the interactions from the adsorbate layers in the junction between the two sections, which are quite thick at those pressures.

We conclude that the adsorption and desorption processes for the simply connected pore model depend on the relative size of the two sections. When this difference is large, adsorption in the narrow section is similar to that in an independent pore with open ends and that in the wide section is similar to the same model with one end closed. When the diameters of the two sections are similar, condensation occurs simultaneously in both sections because the fluid condenses in these sections at almost the same pressure, and evaporation occurs when the menisci recede at both ends of the connected pore resulting in a fused hysteresis loop, which becomes a single loop when the diameters of each section approach each other.

4.2. Pore Model II. In this model (see Figure 2), the end of the narrow section is closed. The dimensions are shown in Figure 8.

The lengths of each section (L_1 , L_2 , and L_3) and the diameter of the wide section (D_1) are kept constant, and the diameter of the narrow section (D_2) is increased from 3.2 to 5.6 nm. The adsorption isotherms for argon at 87.3 K are shown in Figure 9.

As in pore model I, in the adsorption isotherm the two hysteresis loops get closer and merge together when the size difference between the two sections becomes smaller. For the largest difference between the two pore diameters ($D_1 = 6$ nm, $D_2 = 3.2$ nm) hysteresis vanishes altogether. The mechanism of pore filling can be divided into two stages: (i) the advance of the meniscus originating from the closed end of the narrow section is

similar to that for the closed end cylindrical pore;¹⁹ (ii) once the narrow section is filled, the meniscus continues to advance into the wider section toward the pore mouth, and the adsorbed layer in the wider section thickens. When the pore is filled and the pressure is then decreased, molecules are first removed from the positions where they are most weakly held (the central region of the meniscus). The hysteresis loops are much smaller than those for pore model I of the same geometrical dimensions, due to the greater fluid–fluid interactions of an adsorbate when it stays close to the meniscus separating the filled and unfilled sections. Meniscus movement is here the principal mechanism of adsorption and desorption. The schematic illustration of pore filling and pore emptying processes in model II are shown in Figure 10.

4.3. Pore Model III. Here (Figure 11), the wide section is not directly exposed to the bulk surroundings and evaporation of adsorbate from the wide section (cavity) is controlled by the narrow section (neck). The phenomena of cavitation or pore-blocking¹⁵ are expected for these pores. Since the pore models III and IV behave in a very similar way, we shall discuss the evolution of the adsorption isotherm for pore model III in detail and only summarize the results for pore model IV.

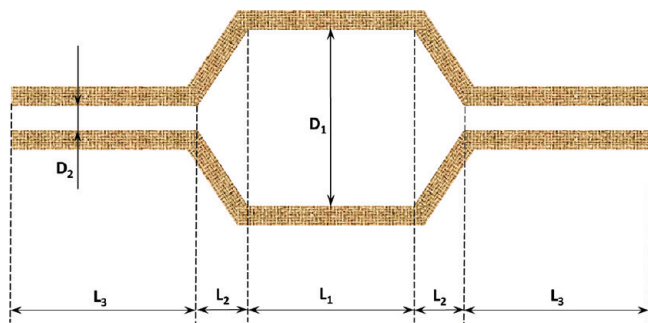


Figure 11. Pore model III.

We study the effects of the relative size of the two sections on the adsorption isotherm by varying the diameter of the narrow section (D_2) from 2.4 to 6.0 nm while the other dimensions are kept constant ($D_1 = 6$ nm, $L_1 = L_3 = 6.81$ nm, and $L_2 = 2$ nm). As seen in Figure 12, the adsorption isotherms can be divided into two groups, which correspond to two distinct evaporation processes, cavitation and pore blocking, both of which have been discussed as possible mechanisms for hysteresis in this type of pore structure. When the neck is smaller than 4 nm (Figure 12A), the adsorption isotherm for this section of the pore is reversible, and there is just one hysteresis loop corresponding to the condensation and evaporation in the cavity; therefore the condensation and evaporation pressures are unaffected by the variation of the neck size. When the neck is larger than 4 nm (Figure 12B), we observe a fused hysteresis loop corresponding to filling and emptying in the neck and the cavity. As the size of the neck approaches that of the cavity, the fused hysteresis loop becomes a single loop as expected for a single cylindrical pore with two open ends. So what is the mechanism of adsorption and desorption that leads to the fused hysteresis loop? Along the adsorption branch, there is a double step condensation corresponding to consecutive condensation processes in the neck and the cavity. As the neck size increases, the condensation pressure in the neck shifts to a higher value and finally merges with that of the cavity, giving rise to a single jump in density. Along the desorption branch, there is a gradual decrease in density, which results when the menisci recede from the ends of the necks, and move toward the interior. Once the density of the liquid bridge has reached its stability limit all the molecules in the bridge evaporate leaving behind layers on the walls of both the necks and the cavity. Upon further reduction in pressure, the adsorption layers are thinned and completely desorb when pressure approaches zero. A fused hysteresis loop has also been observed experimentally for argon adsorption at 87 K in SLN-326 silica, which consists of spherical mesopores of diameter ~ 35 nm connecting through ~ 5 nm worm-like mesopores and additional

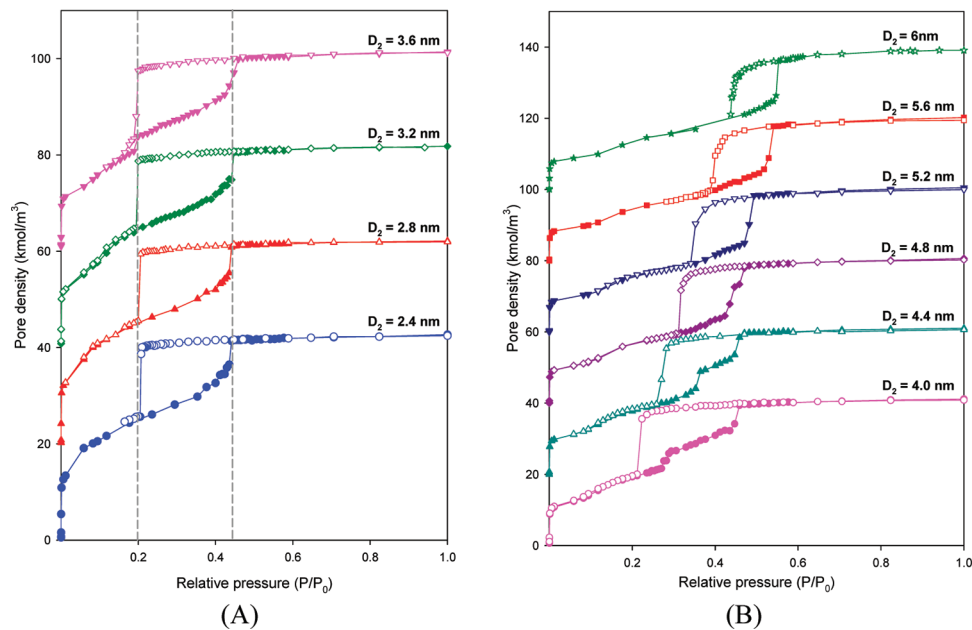


Figure 12. Adsorption isotherm for argon at 87.3 K in pore model III with $D_1 = 6$ nm, $L_1 = L_3 = 6.81$ nm, $L_2 = 2$ nm, and (A) $D_2 = 2.4\text{--}3.6$ nm with the contribution of the wide section and (B) $D_2 = 4.0\text{--}5.6$ nm. Closed symbols represent adsorption branches, and open symbols represent desorption branches. Some adsorption isotherms have been shifted up for clarity.

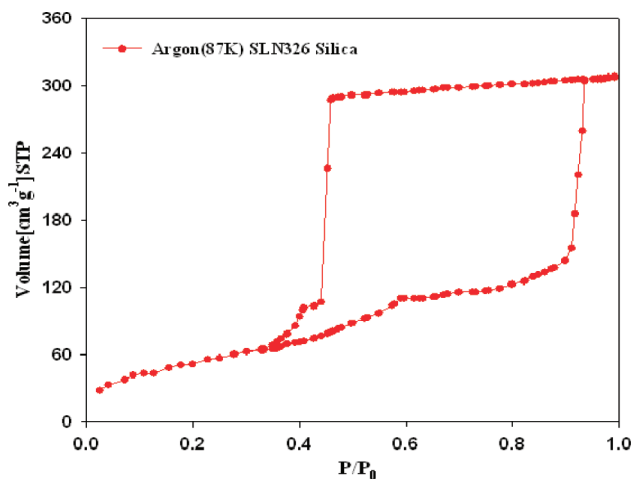


Figure 13. Argon adsorption at 87.3 K in SLN-326 silica, which consists of spherical mesopores of diameter ~ 35 nm that are connected through ~ 5 nm worm-like mesopores and additional micropores.²⁵

micropores (Figure 13).²⁵ Although the adsorbent type and the cavity size are different from our simulation parameters, a similar evaporation mechanism is observed. The neck size of the SLN-326 is larger than 4 nm but still much smaller compared with the cavity; as a result, its hysteresis loop partially merges with that of the cavity to form a fused hysteresis loop, which is similar to the case $D_2 = 3.6$ nm in Figure 12A. Some similar shapes of the hysteresis loop have also been reported for nitrogen adsorption in porous silicon at different temperatures.²⁶

Thus, there is a transition in the evaporation mechanism in a connected pore from cavitation to pore blocking as the pore neck increases. This has also been observed experimentally by Morishige et al.²⁷ when they explored adsorption and desorption isotherms of nitrogen at 77 K on KIT-5 samples with different periods of hydrothermal treatment to expand the neck and cavity sizes (Figure 14). Although the neck and cavity sizes are increased, the mechanism of evaporation is controlled by the pore neck. For the sample hydrothermally treated for only 1 day, the hysteresis loop closed sharply at a relative pressure of 0.47, corresponding to the tensile strength of nitrogen at 77 K, indicating that desorption takes place via cavitation. As hydrothermal treatment time is increased, the evaporation shifted toward higher relative pressures and the evaporation took place more gradually via pore blocking mechanism. Although 5 nm has been suggested to be the critical neck size, it is worthwhile to note that there is no clear distinct boundary between pore blocking and cavitation but rather a gradual transition between them. This is due to the competition between the removal of adsorbate from the receding menisci (pore blocking) and the tension in the stretched fluid in the cavity (cavitation) as the pressure is decreased. This will be clarified in detail by analyzing adsorbate density profile in the later section.

In order to study the difference between the evaporation mechanisms of cavitation and pore blocking, we analyze the density profiles of the pore just before and just after evaporation for two cases: a neck size of 3.2 nm (case A) for cavitation and 4.8 nm (case B) for pore blocking (Figure 15). In case A, since the neck is much smaller than the cavity, the evaporation first occurs in the cavity while the fluid in the neck remains in a stable state (see Figure 15A). This is the cavitation phenomenon. In

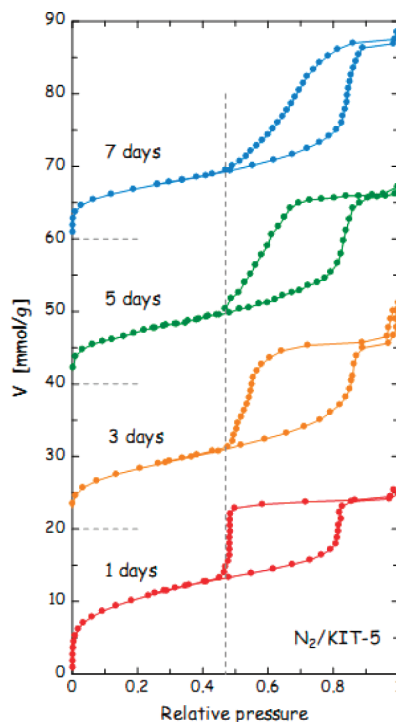


Figure 14. Adsorption–desorption isotherms of nitrogen at 77 K on KIT-5 samples with expanded cavities hydrothermally treated for different periods of time at 393 K. Volumes adsorbed for the samples prepared from the hydrothermal treatment for 3, 5, and 7 days were incremented by 400, 800, and 1200 mL (STP)/g, respectively.²⁷

case B, since the size difference between the two sections is small, desorption is dominated by the two receding menisci; the fluid in the cavity is not stretched to its tensile strength and cavitation does not occur. This is in contrast to case A where the receding menisci only advances partially toward the cavity after the fluid in the cavity has been stretched enough for cavitation to occur. Therefore the distinction between cavitation and pore blocking lies in the competition between removal of adsorbate from the receding menisci and the tension in the stretched fluid in the cavity as the pressure is decreased. When the diameter of the neck relative to that of the cavity is sufficiently small, stretching of fluid in the cavity beyond the limit of its tensile strength is the dominant mechanism and cavitation occurs in the large pore. When the neck size is larger, the menisci recede in the necks, leaving the fluid in the larger pore stretched but intact. The latter mechanism is often described as pore blocking, but it should be noted that the term “pore blocking” is very misleading because the evaporation process does not result in a steep change in density when a certain pressure has been reached, but rather it is a gradual process of receding of menisci from the mouths of the necks.

To study the cavitation and pore blocking phenomena further, we investigate the effects of changing the length of the neck. We chose neck sizes of 3.2 nm (for cavitation) and 4.8 nm (for pore blocking). In Figure 16, we show the adsorption isotherms and snapshots (just before and after the evaporation) for the neck size $D_2 = 3.2$ nm and neck lengths from 1.7 to 6.8 nm. It is seen that the size and the position of the hysteresis loop are unaffected by the length, which is expected because they are governed by the diameters of the cavity. When

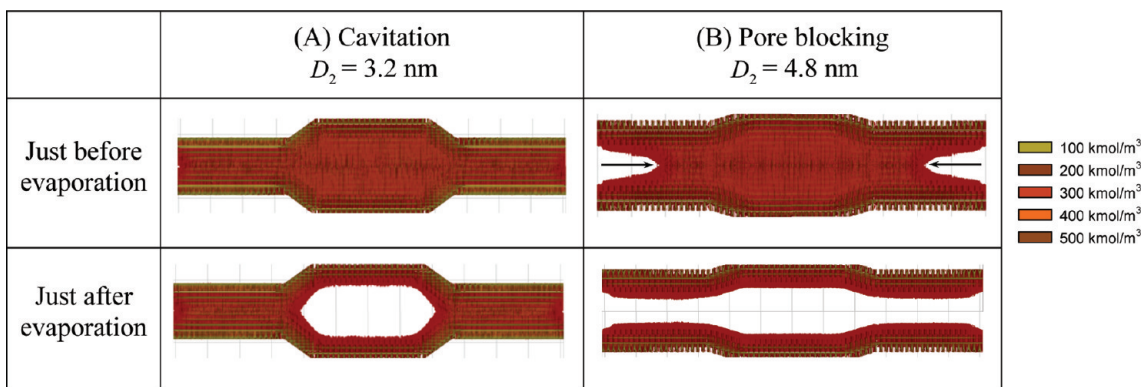
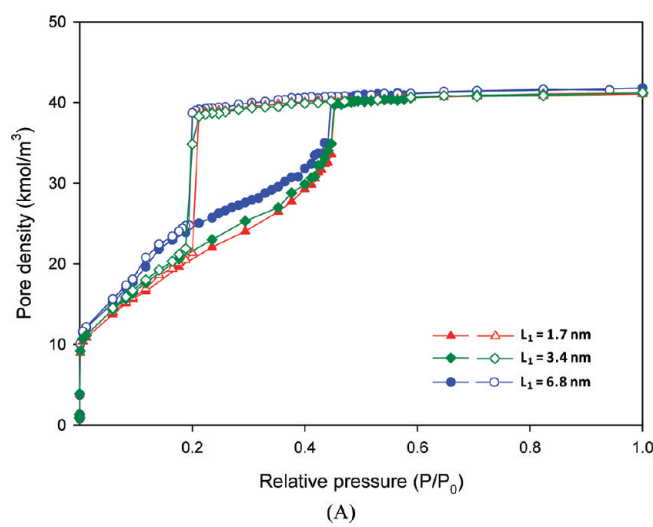
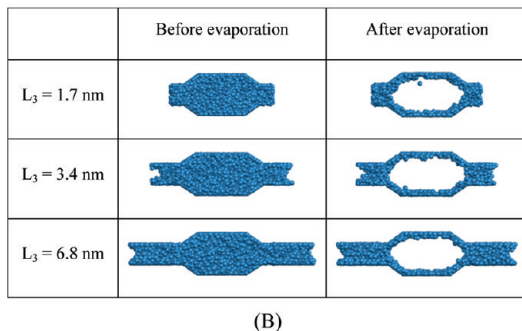


Figure 15. Density profiles of pore model III just before and just after evaporation: (A) cavitation; (B) pore blocking.



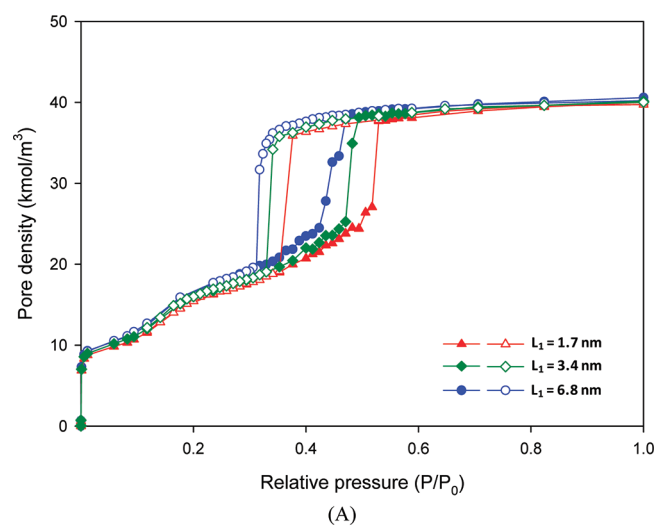
(A)



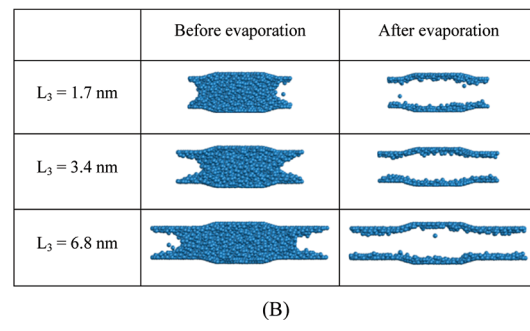
(B)

Figure 16. (A) Adsorption isotherms and (B) snapshots of argon at 87.3 K in pore model III with $D_1 = 6 \text{ nm}$, $D_2 = 3.2 \text{ nm}$, $L_1 = 6.81 \text{ nm}$, $L_2 = 2 \text{ nm}$, and $L_3 = 1.7\text{--}6.8 \text{ nm}$.

$D_2 = 4.8 \text{ nm}$, the “pore blocking” phenomenon is always observed (that is, the receding of the two menisci from the mouths of the necks). The evaporation pressure shifts to a lower value when the length of the small pore is increased due to the longer path that the menisci have to travel within the necks (Figure 17A). Condensation along the adsorption branch of the pore having the longer neck occurs at a lower pressure because there are more solid–fluid interactions per fluid atom in a longer pore, and since the menisci are present at a lower pressure, the cavity fills at a lower pressure compared with



(A)

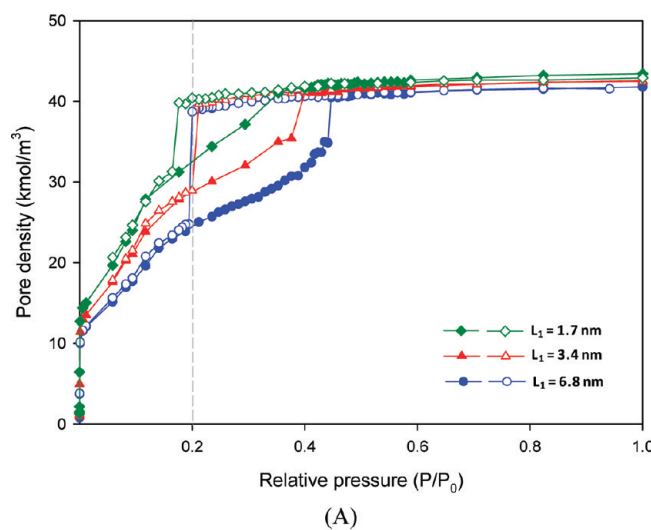


(B)

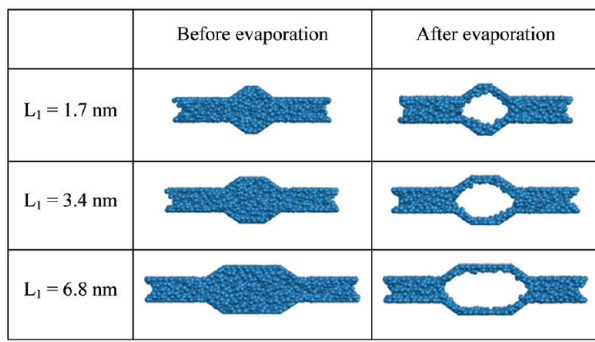
Figure 17. (A) Adsorption isotherms and (B) snapshots of argon at 87.3 K in pore model III with $D_1 = 6 \text{ nm}$, $D_2 = 4.8 \text{ nm}$, $L_1 = 6.81 \text{ nm}$, $L_2 = 2 \text{ nm}$, and $L_3 = 1.7\text{--}6.8 \text{ nm}$.

one connected to pores having shorter necks.¹⁹ Thus, the effects of the neck length on the adsorption isotherm depend on whether cavitation or pore blocking is the operative mechanism. The pressures at which condensation/evaporation occur remain unchanged when there is cavitation, but these pressures shift to lower values with an increase in the neck length when there is “pore blocking”.

We next investigate the length of the cavity. Figure 18 shows the isotherms for a cavity length ranging from 1.7 to 6.8 nm. When the neck size is $D_2 = 3.2 \text{ nm}$, with the exception of the short



(A)



(B)

Figure 18. (A) Adsorption isotherms and (B) snapshots of argon at 87.3 K in pore model III with $D_1 = 6 \text{ nm}$, $D_2 = 3.2 \text{ nm}$, $L_1 = 1.7\text{--}6.8 \text{ nm}$, $L_2 = 2 \text{ nm}$, and $L_3 = 6.8 \text{ nm}$.

neck length ($L_1 = 1.7 \text{ nm}$), the reduced pressure at evaporation is $P/P_0 = 0.2$ because evaporation from the cavity is via a cavitation mechanism and depends on the fluid interactions, independent of the pore properties. When the cavity is very short ($L_1 = 1.7 \text{ nm}$), the evaporation pressure shifts to a lower value due to the influence of the substrate, which stabilizes the confined liquid in the cavity.

The effects of cavity length were also investigated for the neck size of $D_2 = 4.8 \text{ nm}$ (larger than its critical size), where pore blocking is the controlling mechanism for desorption. Figure 19 shows the evolution of adsorption isotherms with an increase in the cavity length. It can be seen that the desorption branch remains unchanged with an increase in the cavity length. Thus, except for the very short pore, an increase in the cavity length does not change the evaporation pressure in this model, irrespective of whether the mechanism is cavitation or pore blocking.

4.4. Pore Model IV. Here (Figure 20), the cavity is not directly exposed to the surrounding but only via a narrower neck, and the pore geometry resembles the ink-bottle that McBain once had on his desk. The mechanism of evaporation from the cavity depends on the neck size of the narrower section. Figure 21 shows the effects of the neck size on the adsorption isotherms of argon at 87.3 K. The cavity size and the length of each section are kept constant ($D_1 = 6 \text{ nm}$, $L_1 = L_3 = 6.81 \text{ nm}$, and $L_2 = 2 \text{ nm}$), and the neck size (D_2) is varied from 2.4 to 5.6 nm. The isotherms can

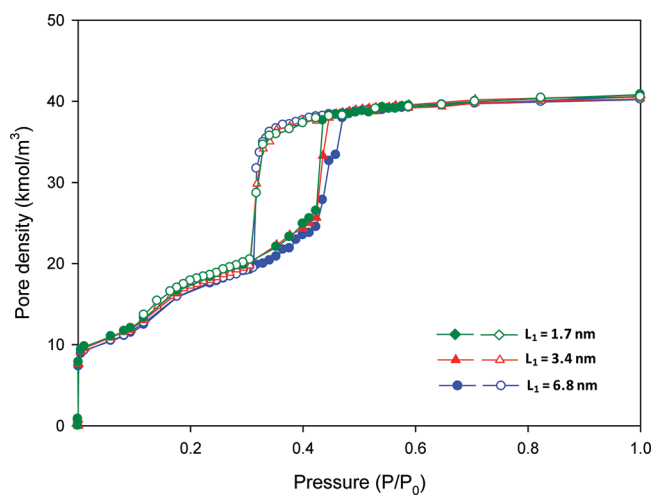


Figure 19. (A) Adsorption isotherms of argon at 87.3 K in pore model IV with $D_1 = 6 \text{ nm}$, $D_2 = 4.8 \text{ nm}$, $L_1 = 1.7\text{--}6.8 \text{ nm}$, $L_2 = 2 \text{ nm}$, and $L_3 = 6.8 \text{ nm}$.

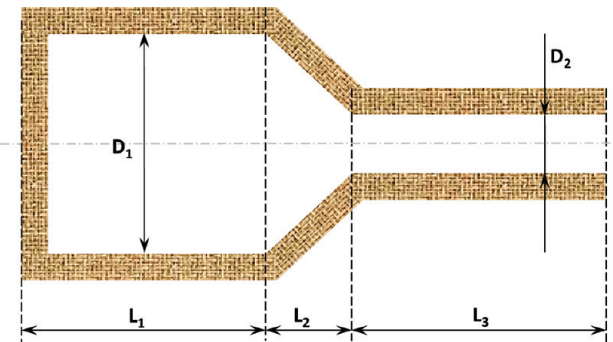


Figure 20. Pore model IV.

again be broadly divided into two groups that correspond to cavitation and pore blocking. The first group is found when the neck is smaller than its critical size ($D_2 < 4 \text{ nm}$), the desorption remains the same and the evaporation occurs at $P/P_0 = 0.2$, which corresponds to the limit of the tensile strength of liquid argon at 87.3 K¹⁹ (Figure 21A). When the narrow section is wider ($D_2 \geq 4.0 \text{ nm}$), the relative pressure at which the evaporation occurs shifts to a higher value with an increase in the neck size (Figure 21B). The explanation follows that discussed earlier for model III. The snapshots of evaporation in these two cases are shown in Figure 22.

5. CONCLUSION

We have presented a systematic study of the adsorption of argon at 87.3 K for different models of a connected pore. For the simple connected pore (pore models I and II), the adsorption isotherm can be described by a combination of simple unit cells, which are independent open-ended and closed cylindrical pores. While the adsorption of the narrow section is almost the same as in the independent cylindrical pore and is not affected by the adsorbate film in the wider section, the adsorption in the wider section is influenced by the narrow section in such a manner that the condensate in the narrow section acts like a closed-end

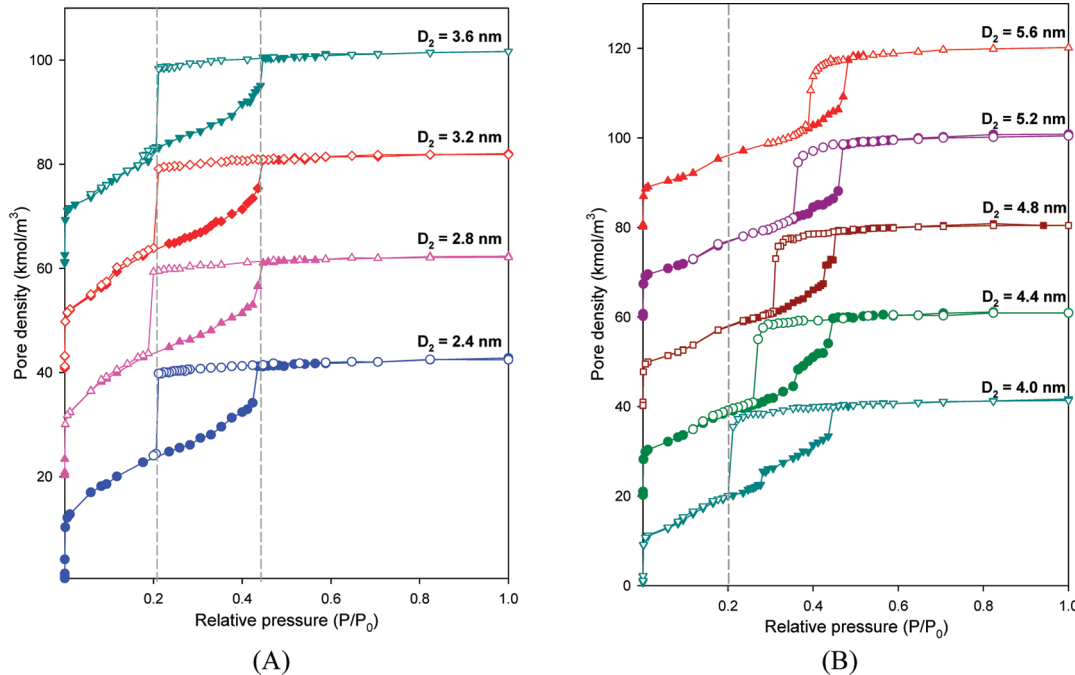


Figure 21. Adsorption isotherm of argon at 87.3 K in pore model IV with $D_1 = 6 \text{ nm}$, $L_1 = L_3 = 681 \text{ nm}$, $L_2 = 2 \text{ nm}$ and (A) $D_2 = 2.4\text{--}3.6 \text{ nm}$ and (B) $D_2 = 4.0\text{--}5.6 \text{ nm}$. Closed symbols represent adsorption branches, while open symbols represent desorption branches. Some adsorption isotherms have been shifted up for a clear observation.

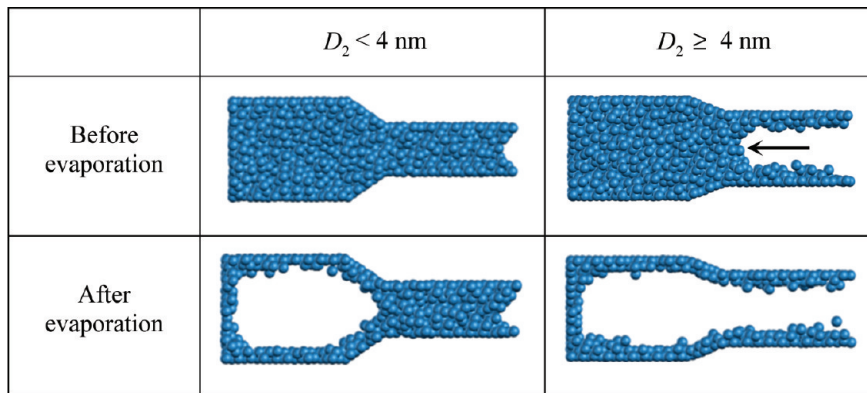


Figure 22. Mechanism of emptying pore model IV.

surface whose affinity depends on the size and structure (open end or closed end) of the narrow section. In the cases where there is a wide cavity connected to surroundings via one or two narrower necks (pore models III and IV), one of two phenomena commonly associated with the ink-bottle model can be recognized: either cavitation or "pore blocking". We find that evaporation from the cavity does not depend on the neck when the neck size is narrower than a critical size (which depends on the adsorbate and the temperature) but is controlled by the condition of the fluid in the neck when the neck diameter is sufficiently large. From analysis of microscopic pictures of the confined fluid in the pore, we conclude that the alternatives of cavitation or pore blocking depend on the mechanism of removal the adsorbate: receding of the menisci in the pore neck or stretching of the fluid in the cavity. If the neck size is sufficiently small, the fluid in the cavity

stretches to the limit of its tensile strength and then cavitates. On the other hand, when the neck size is sufficiently large, the menisci will recede from both ends, and the result will be "pore blocking". Finally, we have explored the effect of neck length and cavity length on cavitation and "pore blocking". It is observed that while the cavity length has negligible effect on the isotherm when the pore is not too short, the influence of the neck length does depend on its diameter. When the neck is smaller than its critical size and cavitation occurs, the adsorption isotherm remains unchanged. When the neck is large enough for pore blocking to occur, the formation and movement of the menisci in the neck become the dominant factors. An increase in neck length then shifts the hysteresis loop to lower relative pressures. This is similar to the behavior found for a finite cylindrical pore with an increase in pore length.¹⁹

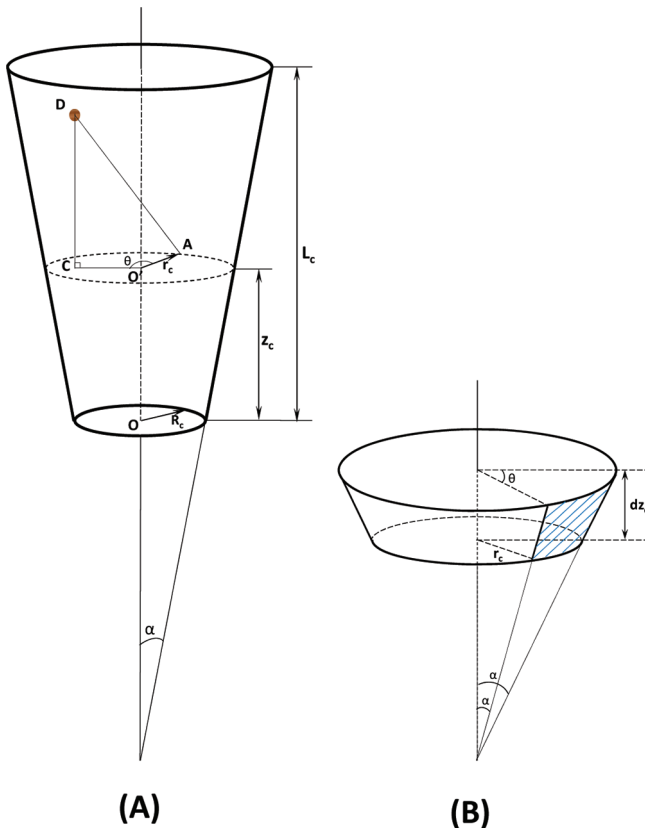


Figure 23. Interaction between a truncated cone and a particle inside the pore (A) and the differential area at the point A (B).

APPENDIX 1

The solid–fluid interaction energy between an adsorbate located at $D(r,z)$ and a truncated cone (Figure 23) in eq 2 is derived as follows.

From the geometry consideration, we have

$$r_c = R_c + z_c \tan \alpha \quad (4)$$

where α is the half angle of the cone.

Therefore, the differential area at the point A is

$$dA = \frac{dz_c}{\cos \alpha} \left[\frac{(R_c + z_c \tan \alpha) d\theta + (R_c + (z_c + dz_c) \tan \alpha) d\theta}{2} \right] \quad (5)$$

Since $dz_c \ll 1$, $z_c \approx z_c + dz_c$ and we have

$$dA = (R_c + z_c \tan \alpha) \frac{dz_c d\theta}{\cos \alpha} \quad (6)$$

Thus, the potential between an adsorbate and all the carbon atoms in the differential A is

$$d\varphi = \left[\rho_s \frac{(R_c + z_c \tan \alpha)}{\cos \alpha} dz_c d\theta \right] \left\{ 4\epsilon_{sf} \left[\left(\frac{\sigma_{sf}}{d} \right)^{12} - \left(\frac{\sigma_{sf}}{d} \right)^6 \right] \right\} \quad (7)$$

or

$$d\varphi = 4\epsilon_{sf} \rho_s \frac{(R_c + z_c \tan \alpha)}{\cos \alpha} dz_c d\theta \sum_{n=3,6} a_n \frac{\sigma_{sf}^{2n}}{(d^2)^n} \quad (8)$$

where $a_3 = -1$ and $a_6 = 1$.

The potential energy between the adsorbate at D and the truncated cone is the integration of the eq 8 with respect to z_c and θ :

$$\begin{aligned} \varphi &= \frac{4\epsilon_{sf} \rho_s}{\cos \alpha} \int_0^{2\pi} \int_{z_c=0}^{z_c=L} (R_c + z_c \tan \alpha) dz_c d\theta \sum_{n=3,6} a_n \frac{\sigma_{sf}^{2n}}{(d^2)^n} \\ &= \frac{4\epsilon_{sf} \rho_s}{\cos \alpha} \sum_{n=3,6} a_n \sigma_{sf}^{2n} \int_0^{2\pi} I(\theta, r, z, n, R_0, L, \alpha) d\theta \end{aligned} \quad (9)$$

where

$$I(\theta, r, z, n, R_0 L, \alpha) = \int_{z_c=0}^{z_c=L} \frac{(R_c z_c \tan \alpha)}{[(z_c - z)^2 + r^2 + z_c^2 - 2r_c \cos \theta]} \quad (10)$$

$$I(\theta, r, z, n, R_0, L, \alpha) = I_1(\theta, r, z, n, R_0, L, \alpha) + I_2(\theta, r, z, n, R_0, L, \alpha) \quad (11)$$

$$\begin{aligned} I_2(\theta, r, z, n, R_0, L, \alpha) &= \frac{(\cos \alpha)^2 \tan \alpha}{2(1-n)} \left\{ \frac{1}{[(L-h)^2 + g]^{n-1}} - \frac{1}{(h^2 + g)^{n-1}} \right\} \\ &\quad (12) \end{aligned}$$

and

$$\begin{aligned} I_1(\theta, r, z, n, R_0, L, \alpha) &= \frac{(\cos \alpha)^2 [R_0 + (\tan \alpha) h(\theta, r, z, \alpha)]}{g^{n-0.5}} [H(x_2, n) - H(x_1, n)] \\ &\quad (13) \end{aligned}$$

where the definition of $H(x, n)$, g , and h are given as below:

$$\begin{aligned} H(x, n) &= \int \frac{dx}{(1+x^2)^n} \\ &= \frac{x}{(2n-1)} \sum_{j=1}^{n-1} \frac{(2n-1)(2n-3)\dots(2n-2j+1)}{2^j (n-1)(n-2)\dots(n-j)(1+x^2)^{n-j}} \\ &\quad + \frac{(2n-3)!!}{2^{n-1}(n-1)!} \arctan(x) \end{aligned} \quad (14)$$

$$\begin{aligned} g(\theta, r, z, R_c, \alpha) &= \cos^2 \alpha (z^2 + r^2 + R_c^2 - 2R_c r \cos \theta) \\ &\quad - \cos^4 \alpha (z + r \tan \alpha \cos \theta - R_c \tan \alpha) \end{aligned} \quad (15)$$

$$h(\theta, r, z, \alpha) = \cos^2 \alpha (z + r \tan \alpha \cos \theta - R_c \tan \alpha) \quad (16)$$

Although eq 9 can be used for any nonzero value of g , it is important that we derive the analytical Taylor series of eq 13 for small values of g because of the singularity of the two terms in the right-hand side of eq 13. Thus, when $0 \leq g \ll 1$, we use

the following Taylor series:

$$I_1(\theta, r, z, 3, R_0, L, \alpha) = -\frac{1}{5} \left[\frac{1}{h^5} - \frac{1}{(h-L)^5} \right] + \frac{3}{7} g^2 \left[\frac{1}{h^7} - \frac{1}{(h-L)^7} \right] - \frac{2}{3} g^4 \left[\frac{1}{h^9} - \frac{1}{(L-h)^9} \right] + \frac{10}{11} g^6 \left[\frac{1}{h^{11}} - \frac{1}{(h-L)^{11}} \right] + o(g^8) \quad (17)$$

$$I_1(\theta, r, z, 6, R_0, L, \alpha) = -\frac{1}{5} \left[\frac{1}{h^5} - \frac{1}{(h-L)^5} \right] + \frac{3}{7} g^2 \left[\frac{1}{h^7} - \frac{1}{(h-L)^7} \right] - \frac{2}{3} g^4 \left[\frac{1}{h^9} - \frac{1}{(L-h)^9} \right] + \frac{10}{11} g^6 \left[\frac{1}{h^{11}} - \frac{1}{(h-L)^{11}} \right] + o(g^8) \quad (18)$$

In our computation, when g is smaller than 10% of the collision diameter of adsorbate, we use the Taylor series in eqs 17 and 18; otherwise, eq 13 is used. This solid–fluid potential energy calculation is valid for a particle either inside or outside of a truncated cone.

ACKNOWLEDGMENT

We acknowledge Australian Research Council for funding this project and the University of Queensland for a research scholarship (to Phuong T. M. Nguyen).

REFERENCES

- (1) Thommes, M. Physical adsorption characterization of ordered and amorphous mesoporous materials. *Nanoporous Materials: Science and Engineering*; Lu, G., Zhao, X. S., Eds.; Imperial College Press: River Edge, NJ, 2004; pp 317–364.
- (2) Cohan, L. H. Sorption hysteresis and the vapor pressure of concave surfaces. *J. Am. Chem. Soc.* **1938**, *60*, 433–435.
- (3) Foster, A. G. Sorption Hysteresis. Part II. The Role of the Cylindrical Meniscus Effect. *J. Phys. Chem.* **1952**, *56*, 1806–1812.
- (4) Cole, M. W.; Saam, W. F. Excitation Spectrum and Thermodynamic Properties of Liquid Films in Cylindrical Pores. *Phys. Rev. Lett.* **1974**, *32* (18), 985.
- (5) Broekhoff, J. C. P.; De Boer, J. H. Studies on pore systems in catalysts XIII. Pore distributions from the desorption branch of a nitrogen sorption isotherm in the case of cylindrical pores. *J. Catal.* **1968**, No. 10, 377–390.
- (6) Broekhoff, J. C. P.; De Boer, J. H. Studies on pore systems in catalysts XII. Pore distributions from the desorption branch of a nitrogen sorption isotherm in the case of cylindrical pores. *J. Catal.* **1968**, No. 10, 368–374.
- (7) Broekhoff, J. C. P.; De Boer, J. H. Studies on pore systems in catalysts IX. Calculation of pore distributions from the adsorption branch of nitrogen sorption isotherms in the case of open cylindrical pores. *J. Catal.* **1967**, No. 9, 8–14.
- (8) Mason, G. The effect of pore lattice structure on the pore-size distributions calculated from sorption isotherms using percolation theory. *J. Colloid Interface Sci.* **1983**, *95* (1), 277–278.
- (9) Mayagoitia, V.; Rojas, F.; Kornhauser, I.; Zgrablich, G.; Faccio, R. J., Two-fold description of percolation in porous media. In *Fundamentals of Adsorption*; LeVan, M. D., Ed.; Kluwer Academic Publishers: Norwell, MA, 1996; pp 595–602.
- (10) Mayagoitia, V.; Rojas, F.; Kornhauser, I. Twofold description of porous media and surface structures: a unified approach to understand heterogeneity effects in adsorption and catalysis. *Langmuir* **1993**, *9* (10), 2748–2754.
- (11) Sarkisov, L.; Monson, P. A. Modeling of adsorption and desorption in pores of simple geometry using molecular dynamics. *Langmuir* **2001**, *17* (24), 7600–7604.
- (12) Everett, D. H. A general approach to hysteresis part 4. An alternative formulation of the domain model. *Trans. Faraday Soc.* **1955**, *51*, 1551–1557.
- (13) Everett, D. H. Adsorption hysteresis. In *The Solid-Gas Interface*; Flood, E. A., Ed.; Marcel Dekker: New York, 1967; Vol. 2, pp 1055–1110.
- (14) Ravikovich, P. I.; Neimark, A. V. Experimental Confirmation of Different Mechanisms of Evaporation from Ink-Bottle Type Pores: Equilibrium, Pore Blocking, and Cavitation. *Langmuir* **2002**, *18* (25), 9830–9837.
- (15) Vishnyakov, A.; Neimark, A. V. Monte Carlo simulation test of pore blocking effects. *Langmuir* **2003**, *19* (8), 3240–3247.
- (16) Ravikovich, P. I.; Neimark, A. V. Density Functional Theory of Adsorption in Spherical Cavities and Pore Size Characterization of Templated Nanoporous Silicas with Cubic and Three-Dimensional Hexagonal Structures. *Langmuir* **2002**, *18* (5), 1550–1560.
- (17) Morishige, K.; Tateishi, N.; Hirose, F.; Aramaki, K. Change in Desorption Mechanism from Pore Blocking to Cavitation with Temperature for Nitrogen in Ordered Silica with Cagelike Pores. *Langmuir* **2006**, *22* (22), 9920–9924.
- (18) Fan, C.; Do, D. D.; Nicholson, D. On the Cavitation and Pore Blocking in Slit-Shaped Ink-Bottle Pores. *Langmuir* **2011**, *27* (7), 3511–3526.
- (19) Nguyen, P. T. M.; Do, D. D.; Nicholson, D. On the Hysteresis Loop of Argon Adsorption in Cylindrical Pores. *J. Phys. Chem. C* **2011**, *115* (11), 4706–4720.
- (20) Do, D. D.; Do, H. D. Effects of potential models in the vapor–liquid equilibria and adsorption of simple gases on graphitized thermal carbon black. *Fluid Phase Equilibr.* **2005**, *236* (1,2), 169–177.
- (21) Bojan, M. J.; Steele, W. A. Computer simulation of physisorption on a heterogeneous surface. *Surf. Sci.* **1988**, *199* (3), L395–L402.
- (22) Steele, W. A. The physical interaction of gases with crystalline solids: I. Gas-solid energies and properties of isolated adsorbed atoms. *Surf. Sci.* **1973**, *36* (1), 317–352.
- (23) Do, D. D.; Do, H. D. Appropriate volumes for adsorption isotherm studies: The absolute void volume, accessible pore volume and enclosing particle volume. *J. Colloid Interface Sci.* **2007**, *316* (2), 317–330.
- (24) Herrera, L.; Do, D. D.; Nicholson, D. A Monte Carlo integration method to determine accessible volume, accessible surface area and its fractal dimension. *J. Colloid Interface Sci.* **2010**, *348* (2), 529–536.
- (25) Rasmussen, C. J.; Vishnyakov, A.; Thommes, M.; Smarsly, B. M.; Kleitz, F.; Neimark, A. V. Cavitation in Metastable Liquid Nitrogen Confined to Nanoscale Pores. *Langmuir* **2010**, *26* (12), 10147–10157.
- (26) Grosman, A.; Ortega, C. Cavitation in Metastable Fluids Confined to Linear Mesopores. *Langmuir* **2011**, *27* (6), 2364–2374.
- (27) Morishige, K.; Tateishi, N.; Hirose, F.; Aramaki, K. Change in Desorption Mechanism from Pore Blocking to Cavitation with Temperature for Nitrogen in Ordered Silica with Cagelike Pores. *Langmuir* **2006**, *22* (22), 9920–9924.